Editors' Suggestion

Clustering and anisotropic correlated percolation in polar flocks

Nikos Kyriakopoulos,[1] Hugues Chaté,[2,3] and Francesco Ginelli[4]
[1]*Department of Applied Physics, Aalto University, 02150, Espoo, Finland*
[2]*Service de Physique de l'Etat Condensé, CEA, CNRS, Université Paris-Saclay, CEA-Saclay, 91191 Gif-sur-Yvette, France*
[3]*Beijing Computational Science Research Center, Beijing 100094, China*
[4]*Department of Physics and Institute for Complex Systems and Mathematical Biology, King's College, University of Aberdeen, Aberdeen AB24 3UE, United Kingdom*

(Received 28 May 2019; published 28 August 2019)

We study clustering and percolation phenomena in the Vicsek model, taken here in its capacity of prototypical model for dry aligning active matter. Our results show that the order-disorder transition is not related in any way to a percolation transition, contrary to some earlier claims. We study geometric percolation in each of the phases at play, but we mostly focus on the ordered Toner-Tu phase, where we find that the long-range correlations of density fluctuations give rise to an anisotropic percolation transition.

DOI: 10.1103/PhysRevE.100.022606

I. INTRODUCTION

Active matter [1] typically involves moving "particles" (such as social animals [2], cells [3,4], biofilaments displaced by motor proteins [5], phoretic colloids [6], etc.). Energy, either stored internally or gathered from the environment, is consumed locally to produce mechanical work. These systems display a wide range of collective phenomena that are not possible in equilibrium. In particular, Toner and Tu have shown that flocking systems such as the celebrated Vicsek model [7], where constant-speed particles locally align their velocities in the presence of noise, can show true long-range orientational order even in two dimensions, in a strongly fluctuating phase endowed by generic anisotropic long-range correlations [8–12].

Active matter systems are also known to often show dense clusters that dynamically form, merge, shrink, and split. This has been observed experimentally in situations as diverse as bacteria colonies [13], actomyosin motility assays [5,14,15], animal groups [16], and active colloidal particles [17]. A wide, power-lawlike distribution of cluster sizes has been reported in certain cases such as gliding myxobacteria [18]. Simple models of self-propelled rods interacting solely via steric exclusion, put forward initially in the context of bacteria, have long been known to exhibit similarly broad distribution of cluster sizes [19–21], a situation sometimes referred to as nonequilibrium clustering. In most of these systems, these clusters are believed to be the consequence of arrested or microphase separation, with size or mass distributions bounded by a finite, albeit sometimes very large, intrinsic cutoff [22,23].

Clusters also appear in flocking models such as the Vicsek model, where they are naturally and unambiguously defined by making use of the finite-range of interactions. Power-law distributions of cluster sizes have also been reported [10,24,25]. Because these observations were mostly made in the region of parameter space where the order-disorder transition takes place, some authors have conjectured that, in active systems exhibiting collective motion, this transition from disorder to ordered collective motion could be somehow generically related to (or even mediated by) nonequilibrium clustering [26]. This claim, at face value, may appear rather surprising: Indeed, in a noisy model such as the Vicsek model, one expects that at large enough density, particles would always form a single, macroscopic, spanning cluster, irrespective of the degree of orientational order present. Conversely, at low enough densities, one has no chance to observe a percolating cluster. It is thus natural to expect a percolation transition [27] separating these two regimes.

Moreover, phase-separation has been recently shown to be at play in dry aligning active matter. It actually provides the best framework to understand the phase diagram of Vicsek-style models [28,29], which contain three phases, with a disordered gas separated from an ordered liquid by a coexistence phase. To the best of our knowledge, it remains unclear whether geometric percolation and the order-disorder transition can interfere in any way in flocking models.

In this work, we come back to this issue, and study clustering phenomena in the Vicsek model, taken here as a prototypical model for dry aligning active matter. Our results show that the order-disorder transition is *not* related in any way to a percolation transition. We study geometric percolation in each of the phases at play, but we mostly focus on the ordered Toner-Tu phase, where we find that the long-range correlations of density fluctuations give rise to an anisotropic percolation transition.

The remainder of this paper is organized as follows: in Sec. II, we summarize the phase diagram of the Vicsek model and recall some of its basic properties. Sections III, IV, and V describe percolation and clustering in the Toner-Tu liquid phase, while we briefly examine the disordered and the coexistence phase in Sec. VI. A discussion and some conclusions can be found in Sec. VII.

II. THE VICSEK MODEL FOR FLOCKING AND ITS PHASE DIAGRAM

We consider the classic version of the Vicsek model [7] with metric interactions in two spatial dimensions. Particles are defined by an off-lattice position $\mathbf{r}_i$ and an orientation $\theta_i \in [0, 2\pi]$, with $i = 1, \ldots, N$. The discrete-time evolution is synchronous: Orientations and positions are updated at integer time steps according to the driven-overdamped dynamics,

$$\theta_i(t+1) = \mathrm{Arg}\left[\sum_{j=1}^{N} \mathcal{A}_{ij}^t \mathbf{v}_j(t)\right] + \eta\,\xi_i(t), \tag{1}$$

$$\mathbf{r}_i(t+1) = \mathbf{r}_i(t) + v_0 \mathbf{v}_i(t+1), \tag{2}$$

where $\mathbf{v}_i = [\cos(\theta_i), \sin(\theta_i)]$ is the unit vector pointing in the direction θ_i, v_0 is the speed of particles, and ξ_i^t is a random angle drawn uniformly in $[-\pi, \pi]$ with δ correlations in space and time. The alignment interaction is limited to a metric range with a radius $r_0 = 1$ [30], and the symmetric and time-dependent interaction matrix $\mathcal{A}^t$ codes for the presence of neighbors within this interaction range:

$$\mathcal{A}_{ij}^t = \begin{cases} 1 & \text{if } ||\mathbf{r}_i(t) - \mathbf{r}_j(t)|| \leqslant 1 \\ 0 & \text{if } ||\mathbf{r}_i(t) - \mathbf{r}_j(t)|| > 1. \end{cases} \tag{3}$$

Effectively, the sum in Eq. (1) runs over all particles in the unit radius disk centered around particle i (i itself included). The finite interaction radius r_0 allows for a natural and unambiguous definition of clusters: Particles within distance r_0 of each other belong to the same cluster. At any given time t clusters are then determined as the connected components of the graph formed by the interaction matrix $\mathcal{A}_{ij}^t$.

We consider square domains of linear size L with periodic boundary conditions, corresponding to a global density $\rho = N/L^2$. In the following, we fix $v_0 = 0.5$ and consider the usual two main control parameters, the global density ρ and the noise amplitude η, the latter playing a role akin to that of temperature in equilibrium systems.

For maximum noise, $\eta = 1$, particle orientations are completely random and decorrelated, so that at each time step their spatial distribution is equivalent to one drawn from a Poisson point process [31]. As the noise is lowered, short-range correlations initially build up (both in orientation and position) and, as a threshold η_{gas} is passed, the system eventually undergoes a spontaneous symmetry breaking phase transition to long-ranged (polar) order, easily characterized by the mean particle orientations order parameter, $\mathbf{V}(t) = \frac{1}{N}\sum_i^N \mathbf{v}_i(t)$.

Active particles move following the orientational degrees of freedom that they themselves carry, linking local order and local density in a simple but highly nontrivial way. As a result, the transition between the fluctuating but *homogeneous* disordered and ordered phases is not direct, like originally thought in analogy with magnetic systems such as the *XY* model, but mediated by a coexistence phase where high-density ordered bands move in a low-density disordered background [10,32–34]. Within the coexistence phase, increasing the global density and/or the system size, the number of traveling bands increases linearly while the residual vapor density between them remains constant [35]. We are thus in the presence of a phase separation scenario: the disordered gas (DG) is separated from the ordered Toner-Tu polar liquid (PL) by a coexistence region with a quantized liquid fraction (the traveling bands are microphases). The corresponding asymptotic phase diagram, following the numerical results of Ref. [35], is reported in Fig. 1. One has thus two transitions, not one, marked by the two binodal lines separating these different phases. They are nondecreasing functions of density, $\eta_{\mathrm{gas}} = \eta_{\mathrm{gas}}(\rho)$, $\eta_{\mathrm{liq}} = \eta_{\mathrm{liq}}(\rho)$, and in the limit of small densities one has $\eta_{\mathrm{gas}} \sim \sqrt{\rho}$ [36]. An inaccessible critical point is pushed towards infinite density [29]. The two transitions are continuous (in the infinite-size limit) but not critical. At finite size, they appear discontinuous because of the large number of particles involved in nucleating a traveling band.

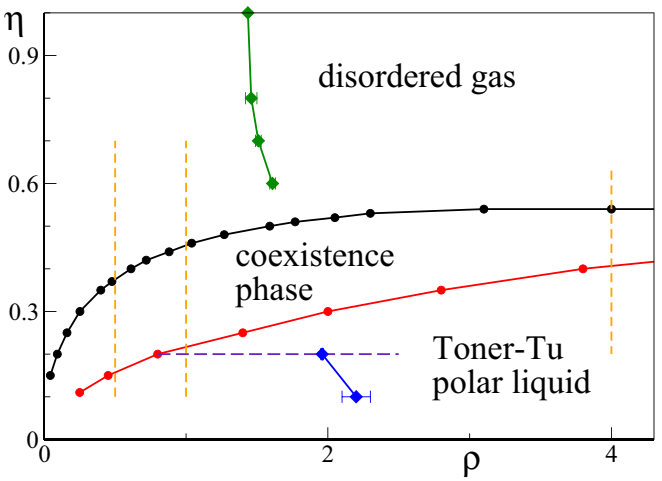

FIG. 1. Phase diagram of the Vicsek model for $v_0 = 0.5$ in the (ρ, η) plane (from Ref. [35]). The binodal line $\eta_{\mathrm{gas}}(\rho)$ separating the disordered gas from the coexistence phase made of traveling high-density high-order bands is reported in black, while the red line marks the liquid binodal $\eta_{\mathrm{liq}}(\rho)$ separating the coexistence region from the Toner-Tu polar liquid. The green line links the diamonds locating the isotropic percolation threshold in the disordered gas phase. The two blue diamonds linked by the solid line show the asymptotic location of the percolation transition in the Toner-Tu liquid phase determined through finite-size scaling (see Sec. IV). The $\eta = 0.2$ horizontal indigo dashed line illustrates the parameter line investigated in detail in Secs. III and IV. The vertical orange lines mark the density values analyzed in Sec. VI.

III. CLUSTERING AND ANISOTROPIC PERCOLATION IN THE TONER-TU LIQUID PHASE

In the following three sections, we focus our attention on the polarly ordered Toner-Tu liquid phase. We initially fix the noise amplitude to $\eta = 0.2$, and study the clustering behavior for different particle densities $\rho > 0.8$, i.e., below the liquid binodal η_{liq} in Fig. 1. Three typical snapshots, obtained in the stationary regime for increasing global densities ($\rho = 1$, $\rho = 1.5$, and $\rho = 1.9$), are shown in Fig. 2 for a system of linear size $L = 256$.

At the lowest density value $\rho = 1$, the largest clusters are clearly smaller than system size. The largest of them contains less than 10% of the total number of particles. The transversal

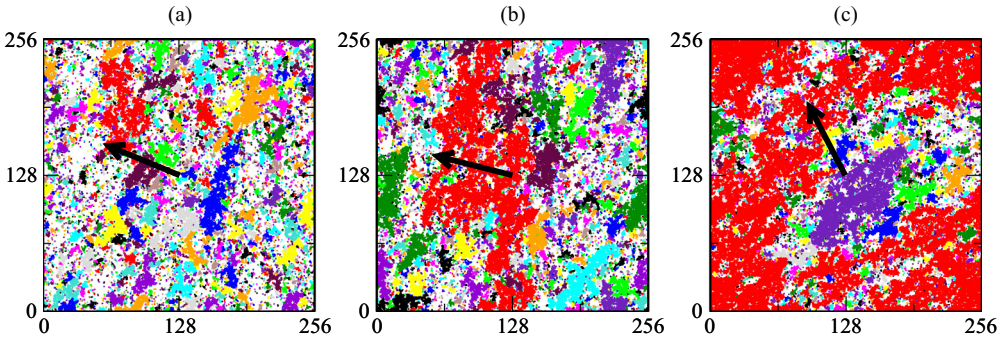

FIG. 2. Typical instantaneous snapshots in the Toner-Tu ordered phase at different densities [(a) $\rho = 1$, (b) $\rho = 1.5$, $\rho = 1.9$]. Other parameters: $v_0 = 0.5$, $\eta = 0.2$. Colors correspond to connected clusters of particles, with the largest cluster in red. Note that due to the large number of different clusters (in the order of thousands in all three panels), each color is used for several distinct clusters, hopefully sufficiently apart from each other to avoid confusion. The thick black arrow marks the instantaneous direction of global order (i.e., the order parameter orientation)

extension (with respect to the current global order direction) of these largest clusters is much larger than the longitudinal one. Increasing the density, clusters remain clearly anisotropic and some of them are spanning across the system along the transversal direction. In the central panel of Fig. 2, one sees a single spanning cluster, comprising less than one-third of the total number of particles. Note that this cluster is not characterized by values of the local density and/or order larger than in the rest of the system, and should therefore not be confused with the fundamentally different traveling bands that characterize the coexistence phase. It is finally only at densities $\rho \gtrsim 1.7$ that the largest cluster starts spanning across all directions, i.e., both transversally and longitudinally. The largest cluster then contains a large majority of all particles, as clearly visible in Fig. 2(c).

This brief graphical inspection suggests that there might be two distinct percolation thresholds, defined by the fact that the largest cluster first spans the system in the direction transverse to global order, and then spans it in all directions. This anisotropy between the transverse and longitudinal directions is not surprising; indeed it is known that the Toner-Tu phase displays anisotropic scaling laws [8]. For instance, the two-point correlation functions of density and velocity fluctuations display generic anisotropic algebraic decay:

$$C(\mathbf{r}) = |\mathbf{r}_\perp|^{2\chi} f(r_\parallel/|\mathbf{r}_\perp|^\zeta), \tag{4}$$

where $\parallel$ and $\perp$ indices, respectively, refer to directions longitudinal and transverse to the mean motion of the flock and the exponents χ and ζ as well as the function f are universal. A notable consequence of this fact is that, in two spatial dimensions, the particles' displacement transversal to the mean velocity is superdiffusive [10,37], while it is simply diffusive in the longitudinal direction (once substracted the mean motion).

We now characterize the percolation transition and its anisotropy from a more quantitative point of view. Individual clusters (labeled by k) can be quantified by their mass s_k, that is, the number of particles in the cluster, and by their linear extension ℓ_k, which we define as twice the in-cluster maximum distance between a cluster particle and the cluster center of mass [38]. The instantaneous maxima of these quantities are, respectively, $s_M = \max_k(s_k)$ and $\ell_M = \max_k(\ell_k)$ where the cluster index k runs over all clusters of a given configuration.

Two order parameters are routinely employed in the literature [39] about isotropic percolation problems, the (normalized) mean largest cluster-size n and the mean cluster maximum linear extension d, where the average is taken over many different realizations (e.g., sampling a long trajectory in the stationary state at regular time intervals). The definitions of n and d and the associated standard deviations σ_n and σ_d read

$$n \equiv \frac{\langle s_M \rangle}{N}, \quad \sigma_n \equiv \frac{\sqrt{\langle (s_M - \langle s_M \rangle)^2 \rangle}}{N}, \tag{5}$$

$$d \equiv \frac{\langle \ell_M \rangle}{\sqrt{2}L}, \quad \sigma_d \equiv \frac{\sqrt{\langle (\ell_M - \langle \ell_M \rangle)^2 \rangle}}{\sqrt{2}L}. \tag{6}$$

In our anisotropic situation, n and d are expected to behave differently as the density is increased, with d rising earlier to order 1 values and n following later. This is indeed observed in Fig. 3(a) where the two indicators are compared for a system of size $L = 256$ and $\eta = 0.2$. The standard deviations σ_n and σ_d peak at two different density values [Fig. 3(b)].

We also investigated directly the spanning probability S, i.e., the probability that a spanning cluster does appear. While, in the thermodynamic limit, $S(\rho)$ is a step function with the jump exactly located at the phase transition, in finite systems $S(\rho)$ is smoothed around the (finite-size) percolation point [27]. To take into account anisotropy, we consider both a transversal and a longitudinal spanning probability, $S_\perp$ and $S_\parallel$, defined, respectively, as the probability that a cluster wraps around the $L \times L$ torus in the transversal or longitudinal (with respect to the order parameter $\mathbf{V}$) directions [40]. (We discuss the accuracy of these measures in finite systems—where fluctuations lead to the diffusion of the instantaneous mean orientation of motion $\mathbf{V}(t)$—in the next section.) For the moment, we simply note that the transversal spanning probability $S_\perp$ rises from zero toward one earlier than the longitudinal probability $S_\parallel$, as shown in Fig. 3(c).

Before concluding this section, we note that a reliable numerical evaluation of the above configuration averages—as the one presented in Fig. 3—is considerably more difficult to obtain than in standard percolation problems, where the

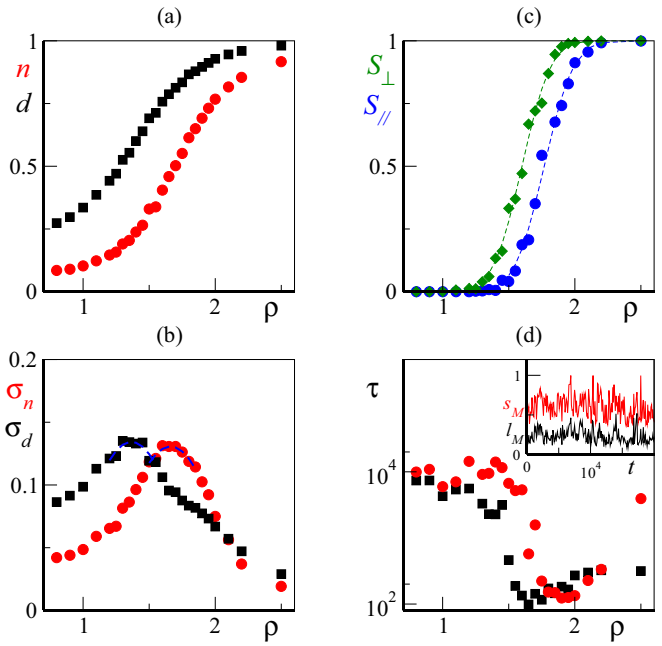

FIG. 3. Anisotropic percolation transition in the Toner-Tu ordered phase. (a) Normalized mean largest cluster-size n (red dots) and normalized mean cluster maximum linear extension d (black squares) as a function of the global density ρ. (b) Corresponding standard deviations σ_n (red dots) and σ_d (black squares). The blue dashed lines show quadratic fits of the peak regions (see text). (c) Transversal ($S_\perp$) and longitudinal ($S_\parallel$) spanning probabilities as a function of total density. The dashed lines show a fit based on the error function (see text). (d) Autocorrelation time τ of the time series of maximal cluster-size s_M (red dots) and maximal linear extension ℓ_M (black squares) as a function of global density. Inset: typical excerpts from these time series for $\rho = 1.5$. Other parameters: $L = 256$, $\eta = 0.2$, and $v_0 = 0.5$. Configurations averages have been computed sampling every 100 time steps a $T = 10^6$ time series in the stationary regime. The standard error (see text) of the data shown in panels (a–c) is equal or smaller than the symbol size.

probability distribution of the particle positions is exactly known and the system configurations can be generated from it. In our case, on the contrary, one has to generate sufficiently uncorrelated configurations from the dynamics. This requires first to evolve the system from some initial condition into the stationary state (which for large systems may require a considerable number of timesteps). Then, to obtain configuration averages, one has to take averages over timescales T much larger than the typical autocorrelation time. Consider for instance the time series of s_M and ℓ_M discussed above [an example of which for $\rho = 1.5$ is shown in the inset of Fig. 3(d)]. For the above parameters $L = 256$ and $\eta = 0.2$, the typical autocorrelation time τ [41] in the low-density regime is of the order of 10^4 time steps. Note, however, that near the percolation transition τ drops suddenly by almost two orders of magnitude. This could seem counterintuitive, as phase transitions are typically associated with a slowing down of the dynamics. However, one has to realize that near the percolation transition one has a wide distribution of competing clusters with sizes close to the spanning threshold, so that relatively small configuration changes may promote a different cluster to the largest cluster status (either in total mass or linear extension) thus resulting in a dramatic drop in the autocorrelation time for s_M and ℓ_M.

Once the autocorrelation time has been estimated, the accuracy of the empirical averages can be evaluated by the standard error $\sigma/\sqrt{T/\tau}$, where σ is one standard deviation and T/τ the number of independent configurations.

IV. FINITE-SIZE SCALING ANALYSIS OF PERCOLATION IN THE TONER-TU LIQUID PHASE

One of the best ways to numerically investigate critical phase transitions is to perform a finite-size-scaling (FSS) study, measuring the lowest moments of suitable order parameters as the system size is systematically increased. This is a classical approach in statistical physics, routinely applied to study both equilibrium and out-of-equilibrium critical phase transitions [42], and it has been already applied to the study of the percolation transition, for instance, bond percolation on square lattices [27,43]. The main difficulty, generally, is to be sure to probe system sizes large-enough so that one is in the scaling regime.

A. Percolation in the longitudinal direction

We first concentrate on the longitudinal percolation transition, i.e., the point at which the spanning cluster becomes two-dimensional and starts to span also in the broken symmetry direction.

The mean largest cluster-size n is associated with the probability n/N that an arbitrary particle belongs to the largest cluster. In percolation theory, it is known to follow the finite-size scaling relation [43]

$$n = L^{-\beta/\nu} f\big((\rho - \rho_c^\infty)L^{1/\nu}\big), \tag{7}$$

where f is a scaling function and β and ν two universal critical exponents. At $\rho = \rho_c^\infty$, the asymptotic critical point, $f(0) =$ const. and one obtains the power-law behavior $n \sim L^{-\beta/\nu}$. In two-dimensional standard percolation, one has $\nu_p = 4/3$ and $\beta_p = 5/36$ [44] (and thus $\beta_p/\nu_p = 5/48$).

By systematically changing the density ρ and the system size between $L = 64$ and $L = 1024$, we find [see Fig. 4(a)] that for $\rho_c^\infty \approx 1.95$ the mean largest cluster size indeed follows a power-law decay with an exponent compatible (our best fit being $\beta/\nu = 0.108(5)$) with the standard percolation value of $\beta_p/\nu_p = 5/48 \approx 0.104$.

Another independent exponent can be deduced from the finite-size scaling of the maximum of the susceptibility $\chi_n \equiv L^2\sigma_n^2$,

$$\chi_n^M = L^{-\gamma/\nu}, \tag{8}$$

with—for $d = 2$ standard percolation—$\gamma_p = 43/18$ [44], so that $\gamma_p/\nu_p = 43/24$. For each system size L we estimate the peak susceptibility χ_M by a quadratic fit of the peak region of $\sigma_n(\rho)$. In Fig. 4(b) we show that once again our numerical estimates are in very good agreement with the standard percolation exponent. Indeed, our best fit of $\gamma_\parallel/\nu_\parallel = 1.83(5)$ is fully compatible with the standard percolation value of $43/24 \approx 1.79$.

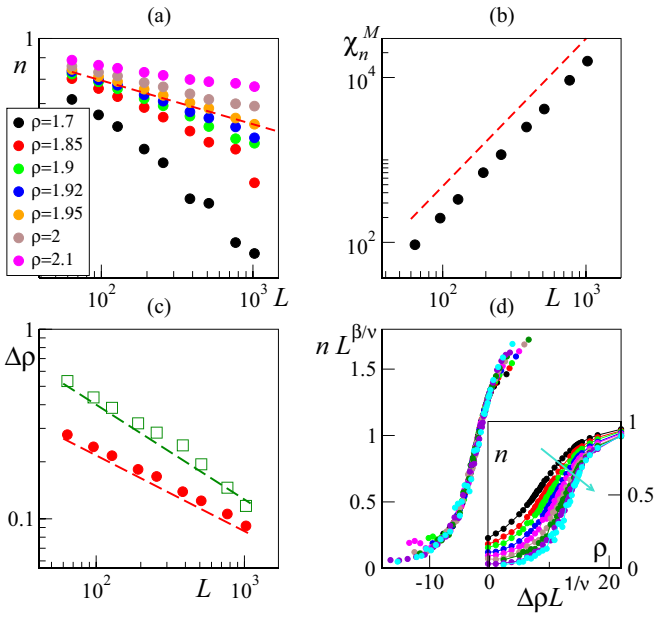

FIG. 4. Finite-size scaling analysis of the percolation transition in the Toner-Tu ordered phase. (a) Mean largest cluster-size n vs system size L for different densities (see legends). The dashed red line marks the standard percolation critical exponent ratio $\beta_p/\nu_p = 5/48$. (b) Susceptibility peak value (black dots) χ_n^M vs system size L. The dashed red line marks the standard percolation critical exponent ratio $\gamma_p/\nu_p = 43/24$. (c) Critical point location finite-size corrections $\Delta\rho = \rho_c^\infty - \rho_c(L)$ evaluated either from the midpoint of the spanning probability S_2 (red full dots) or from the peak location of the standard deviation $\sigma_n(\rho)$ (green empty squares). Here we have used $\rho_c^\infty = 1.96$. The dashed red line marks a power-law decay with an exponent -0.4, while the dashed green line falls off as $L^{-0.5}$. (d) Data collapse of n according to the scaling relation Eq. (7) with $\rho_c^\infty = 1.96$ and exponents $\beta = \beta_p = 5/36$, $1/\nu_\perp = 0.4$ for different system sizes between $L = 64$ and $L = 1024$. Inset: Noncollapsed curves. From top to bottom: $L = 64$, $L = 96$, $L = 128$, $L = 192$, $L = 256$, $L = 384$, $L = 512$, $L = 768$, and $L = 1024$. Other parameters are $\eta = 0.2$ and $v_0 = 0.5$. As in Fig. 3, averages have been computed sampling a 10^6 time-steps-long time series every 100 time steps. The standard error (see text) of the data shown in panels (a)–(c) is equal or smaller than symbol size.

We are left with the estimation of the correlation exponent ν that determines finite-size corrections to the critical point,

$$\Delta\rho \equiv \rho_c^\infty - \rho_c(L) \sim L^{-1/\nu}. \tag{9}$$

Here we adopt and compare two different estimates for the finite-size critical density $\rho_c(L)$. We first estimate it as the location ρ_M of the maximum of the largest cluster-size standard deviation $\sigma_n(\rho)$ (once again, evaluated through a quadratic fit of the peak region). Our results, illustrated in Fig. 4(c) (green squares) essentially confirm our previous estimate for the asymptotic critical point, $\rho_c^\infty = 1.96(1)$. However, finite-size corrections decay slower than expected for standard percolation in two dimensions, and we have $1/\nu_\parallel \approx 0.5$. It has to be noted that this estimate is based on a second moment (the standard deviation), so that its reliability could be questioned.

A second and perhaps more accurate estimate of the finite-size critical density can be obtained measuring the density value by which the finite-size spanning probability crosses 1/2. We are here interested in the longitudinal spanning probability $S_\parallel$. Measuring it in relatively small systems, where the mean orientation $\mathbf{V}(t)$ strongly diffuses in its angular component, can be, however, a difficult task. The central limit theorem implies that the mean orientation should diffuse with an angular diffusion constant proportional to η^2/N. For small enough system sizes, thus, the mean orientation can change faster than the time needed by clusters to realign transversally with respect to $\mathbf{V}(t)$. Therefore, in our FSS analysis we prefer to consider, instead of the transversal and longitudinal spanning probabilities, the one and two-dimensional spanning probabilities S_1 and S_2. The former is the probability that a cluster spanning along at least one spatial direction (i.e., to join two opposite sides of the system) does exist. The latter probability, however, requires the spanning cluster to wrap along both spatial directions, that is to join all four sides of our system. Numerical simulations show that—at least in the parameter range we are interested in—for $L \gtrapprox 256$ we have to a good accuracy $S_\perp \approx S_1$ and $S_\parallel \approx S_2$. For smaller system sizes, however, we have $S_1 < S_\perp < S_\parallel < S_2$.

In the following, we estimate the finite-size critical density as the density value by which an error function based fit [45] of the finite-size spanning probability $S_2(\rho)$ crosses 1/2 [see Fig. 6(a)]. This second estimate, reported by full red circles in Fig. 4(c), also points toward $\rho_c^\infty = 1.96(1)$ but with an even slower decay of finite-size corrections, $1/\nu_\parallel \approx 0.4$.

Altogether, our estimates for the critical exponent $\nu_\parallel$ are clearly different from standard percolation in $d = 2$, $\nu_p = 4/3$. Combining our two different approaches we get $\nu_\parallel = 2.2(3)$, with the upper limit $\nu_\parallel \approx 2.5$ being suggested by the slightly more reliable spanning probability estimates. An estimate exclusively based on the latter estimate would return $1/\nu_\parallel = 0.40(2)$ and $\nu_\parallel = 2.5(1)$.

This value for the critical exponent $\nu_\parallel$, different from the one of standard percolation, is indeed confirmed by attempting a data collapse of the mean largest cluster-size n according to the scaling relation Eq. (7). Our data clearly rule out the value $\nu_p = 4/3$, and we obtain a satisfactory collapse with $\beta_\parallel/\nu_\parallel = \beta_p/\nu_p = 5/48$ and $1/\nu_\parallel$ in the range $0.4 \sim 0.5$.

Also note that our asymptotic critical density $\rho_c^\infty = 1.96(1)$ is significantly larger than the asymptotic critical density for standard continuum percolation: In two spatial dimensions, the most accurate estimate for the continuum percolation threshold for noninteracting, fully penetrable disks of radius r randomly distributed according to a Poisson point process (PPP) corresponds to a critical area $A_c = \pi r^2 \rho_c^{\mathrm{PPP}} = 1.2808737(6)$ [46]. Since a unit interaction radius corresponds to a disk radius $r = 1/2$, we have $\rho_c^{\mathrm{PPP}} = 1.43632545(9)$.

B. Harris criterion for percolation in correlated density fields

While a shift in the critical percolation point is not surprising in the presence of activity, and indeed has been observed before in disordered active matter systems [39], the significant difference between our estimate for the critical exponent ν and the standard percolation value ν_p deserves a few more comments.

It is indeed known that long-range correlations in the particle density can change the value of the critical exponent ν.

In the percolation literature, this is known as the Harris criterion [47,48]: In the presence of sufficiently long-ranged density correlations,

$$C_\rho(r) \sim r^{-\alpha} \quad \text{with} \quad \alpha < \frac{2}{\nu_p}, \tag{10}$$

finite-size corrections are indeed stronger and the exponent ν takes larger values,

$$\nu = \nu_H = \frac{2}{\alpha}. \tag{11}$$

However, for correlations decaying faster, $\alpha > 2/\nu_p$, correlations are not relevant and usual finite-size corrections apply, $\nu = \nu_p$.

Applying the Harris criterion to our results suggests that the density field correlation should decay with a power law with an exponent $\alpha = 2/\nu_\parallel$ in the range $0.8 \sim 1$. Using only the estimate derived from the spanning probability distributions, we would have $\alpha = 0.80(4)$.

We recall that the Toner-Tu phase is endowed with long-range density correlations [8,37]. Their exact real space expression, however, is not known explicitly, so that here we resort to estimate them numerically in the range of sizes accessible to the present FSS analysis. While it is known that correlations are stronger in the transversal than in the longitudinal direction, the numerical measure of anisotropic correlations is a challenging issue. Restricting the measure either in the transversal or longitudinal directions greatly reduces the available statistics and suffers from problems due to the angular diffusion of the mean direction of motion analogous to the one discussed in the previous section. However, one can expect that the onset of a cluster percolating in both directions (as measured by the spanning probability S_2) could be well captured by measures of density correlations averaged over all spatial directions. In the following, therefore, we focus on isotropic correlations of density fluctuations

$$C_\rho(r, L) = \langle\langle \delta\rho(\mathbf{x}+\mathbf{r}, t)\, \delta\rho(\mathbf{x}, t)\rangle_S\rangle_t, \tag{12}$$

where $r = |\mathbf{r}|$ and $\delta\rho(\mathbf{x}, t) \equiv \tilde{\rho}(\mathbf{x}) - \rho$ are the local density fluctuations of a suitably coarse-grained density field $\tilde{\rho}(\mathbf{x})$, and $\langle\cdot\rangle_S$ indicates an average over the spatial coordinate $\mathbf{x}$ and the orientations of the displacement $\mathbf{r}$. Isotropic correlations are then further averaged in time, with $\langle\cdot\rangle_t$ indicating an average over stationary state configurations. A more detailed analysis of anisotropic correlations will be reported in Ref. [49].

The scaling of correlations is expected to be the same in the entire Toner-Tu phase. Here we focus on a point close to the percolation threshold, $\eta = 0.2$ and $\rho = 1.9$, but we have verified that the behavior for lower or higher densities stays the same. Our numerically determined correlations are shown in Fig. 5(a). Note that in finite systems the spatially integrated fluctuations vanish by construction $\int d\mathbf{x}\delta\rho(\mathbf{x}, t)$, and this implies that the correlation function $C(r, L)$ should have at least one zero (as there are surely anti-correlated regions). The smallest value of r for which correlations vanish can be taken as a measure of the correlation length ξ, that is $C(\xi, L) = 0$. Moreover, in systems where a continuous symmetry is spontaneously broken correlations are known to be scale free, i.e., $\xi \sim L$ [see inset of Fig. 5(a)] and $C(r) \sim r^{-\alpha}$ in the thermodynamic $L \to \infty$ limit. Finite-size correlations

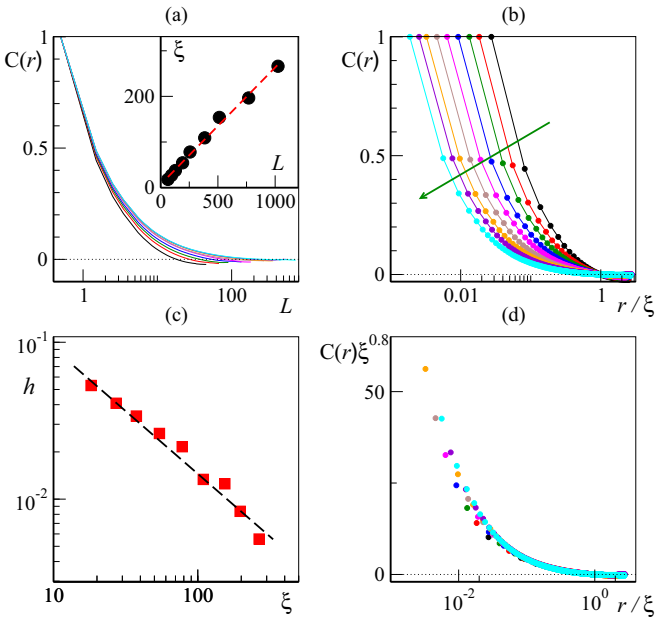

FIG. 5. (a) Isotropic density fluctuations correlation function in the Toner-Tu ordered phase ($v_0 = 0.5$, $\eta = 0.2$, $\rho = 1.9$) and increasing system sizes, $L = 64, 96, 128, 192, 256, 384, 512, 768, 1024$ (from bottom to top). Inset: Correlation length ξ as a function of system size L. The dashed red line marks our best linear fit. (b) Same as (a) but after rescaling of the space variable. System size increases along the green arrow. (c) Finite-size scaling of the (negative) slope h (see text). The dashed black line marks a power-law decay with exponent $-\alpha = -0.8$. (d) Data collapse according to Eq. (16). Correlation functions have been averaged over 10^4 different spatial configurations, sampled from the stationary state dynamics every 10^2 time steps. Standard errors are of the size of the symbols or smaller.

are thus taken into account by [11]

$$C_\rho(r, L) = r^{-\alpha}\, g\left(\frac{r}{\xi}\right), \tag{13}$$

where the scaling function obeys $g(u) = 0$ for $u = 1$ and $g(u) \to$ const. for $u \to 0$.

The isotropic correlation exponent α can be determined by finite-size analysis. Let us choose the rescaling $y = r/\xi$. From Eq. (13), we have [see Fig. 5(b)]

$$C_\rho(y, L) = y^{-\alpha}\xi^{-\alpha} g(y). \tag{14}$$

From Eq. (14) it follows that a finite-size analysis of the (negative) slope h of the rescaled correlation function evaluated in $y = 1$ can be used to estimate the correlation exponent,

$$h = -\frac{d}{dy} C_\rho(y, L)|_{y=1} = \xi^{-\alpha}|g'(1)| \sim \xi^{-\alpha}. \tag{15}$$

Our best numerical estimates, reported in Fig. 5(c), are indeed compatible with the correlation value suggested by the Harris criterion, $\alpha \approx 0.8$.

Moreover, as illustrated in Fig. 5(d), once the correlation exponent has been determined, the finite-size correlation functions can be collapsed to a size independent universal

curve

$$C_\rho^R(y) \equiv \xi^{-\alpha} C_\rho\left(\frac{r}{\xi}, L\right). \tag{16}$$

Our brief analysis of density correlations shows that the anomalous finite-size corrections exponent ν we have measured for our percolation transition (especially through the more reliable spanning probabilities measures) is fully compatible with the one expected by the Harris criterion for correlated percolation.

We finally note that also the critical exponents β and γ may be modified by sufficiently strong correlations. However, it has been verified numerically [44] that the hyperscaling relation of standard percolation,

$$\nu_p d_s = 2\beta_p + \gamma_p \tag{17}$$

(with d_s being the spatial dimension), is still verified by the correlated Harris exponents

$$\nu_H d_s = 2\beta_H + \gamma_H. \tag{18}$$

Interestingly, we find that this latter hyperscaling relation is also verified by our data: As we have seen, our two-dimensional estimates for the ratios β/ν and γ/ν are both compatible with the values expected by standard correlation theory, so that

$$2\frac{\beta}{\nu} + \frac{\gamma}{\nu} = 2.05(6). \tag{19}$$

C. Percolation in the transversal direction

We finally discuss the percolation transition taking place in the transversal direction. Repeating the procedure outlined for the longitudinal percolation transition, we evaluate the finite-size transversal percolation threshold density $\rho_t(L)$ from the behavior of the one-dimensional spanning probability S_1 [see Fig. 6(b)]. Our best estimates are reported in the top panel of Fig. 6(c) (black squares) together with the ones for the finite-size longitudinal percolation critical density $\rho_c(L)$ (red circles). Quite interestingly, our numerical results indicate that their difference $\Delta_{ct}(L) \equiv \rho_c(L) - \rho_t(L)$ [blue triangles in the lower half of Fig. 6(c)] seems indeed to vanish in the limit of large L, suggesting that in the thermodynamic limit $\rho_t(L) \to \rho_c^\infty = 1.96(1)$ and percolation takes place simultaneously in both directions.

Finite-size effects, however, seem to be stronger in the transversal direction, with a slower decay of finite-size corrections,

$$\Delta\rho_t(L) \equiv \rho_t(L) - \rho_c^\infty \sim L^{-1/\nu_\perp}. \tag{20}$$

This can be deduced from the lower panel of Fig. 6(c), where $\Delta\rho_t(L)$ (black squares) exhibits a power-law decay compatible with an exponent $1/\nu_\perp \approx 0.3$, suggesting $\nu_\perp \approx 3.3$.

Going beyond transversal finite-size effects, however, we notice that the cluster maximum linear extension d seems to show rather anomalous scaling properties. As it can be readily deduced from the inset of Fig. 6(d), its finite-size curves do cross near the critical density. This implies that its scaling relation should take the form

$$d = f_\perp\left[(\rho - \rho_c^\infty)L^{1/\nu_\perp}\right], \tag{21}$$

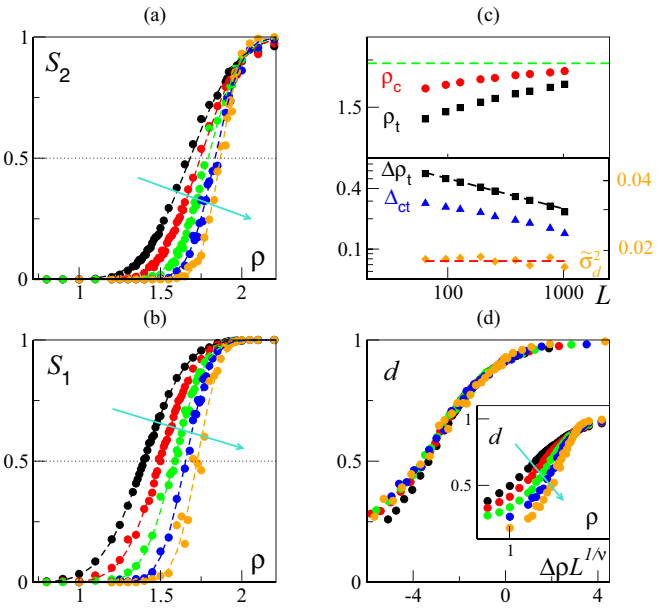

FIG. 6. (a), (b) Two- and one-dimensional spanning probabilities S_2 and S_1 as a function of global density ρ for different system sizes ($L = 64, 128, 256, 512, 1024$, increasing along the cyan arrow. Dashed lines are fits by the error function [45], while the horizontal dotted line shows the threshold probability $1/2$ used to define the finite-size percolation point (see text). (c) Top panel: Transversal (black squares) and longitudinal (red circles) finite-size percolation densities as a function of system size L. The horizontal green line marks our best estimate for the asymptotic percolation point $\rho_c^\infty = 1.96$. (c) Bottom panel: Transversal percolation point finite-size corrections $\Delta\rho_t = \rho_c^\infty - \rho_c(L)$ (black squares), longitudinal to transversal finite-size difference Δ_{ct} (blue triangles, see text) and maximum variance of the largest cluster linear extension $\tilde{\sigma}_d^2$ as a function of system size L in a double logarithmic scale. The dashed black line marks a power-law decay with an exponent 0.3, while the red one corresponds to constant behavior. (d) Data collapse of the mean maximum cluster extension d according to the scaling relation Eq. (21) with $\rho_c^\infty = 1.96$ and $1/\nu_\perp = 0.3$ for different system sizes between $L = 64$ and $L = 1024$ [color coded as in panels (a) and (b)]. In the inset: Noncollapsed curves for the mean largest cluster-size L vs density ρ. Along the cyan arrow: $L = 64, 128, 256, 512, 1024$. System parameters and simulation statistics as described in the caption of Fig. 4.

with $f_\perp$ a transversal scaling function. As we show in Fig. 6(d), one can indeed make use of this scaling relation to achieve a satisfactory collapse of the $d(\rho)$ curves by only rescaling them along the abscissas. Comparison with the general scaling form Eq. (7) thus implies the rather singular $\beta_\perp = 0$.

Finally, we discuss the γ exponent, associated to the maximum linear extension susceptibility

$$\chi_d \equiv L^2\sigma_d^2, \tag{22}$$

whose peak value is expected to scale as

$$\chi_d^M \sim L^{\gamma_\perp/\nu_\perp}. \tag{23}$$

Assuming that an hyperscaling relation analogous to Eq. (17) still holds between the transversal exponents, in two spatial

TABLE I. Longitudinal and transversal percolation exponents compared with the ones of standard percolation theory. Longitudinal exponents are particularly difficult to evaluate due to strong finite-size effects and ours are rough estimates. For this reason we are not confident in providing precise uncertainty estimates.

	$1/\nu$	β/ν	γ/ν
Standard percolation, $d_s = 2$	3/4	5/48	43/24
Longitudinal percolation	0.44(6)	0.108(5)	1.83(5)
Transversal percolation	0.3	0	2

dimensions we would get $\gamma_\perp/\nu_\perp \approx 2$. By virtue of Eq. (22), this in turn implies that also the peak variance of the largest cluster linear extension should not scale with system size,

$$\tilde{\sigma}_d^2(L) \equiv \max_\rho \sigma_d^2(\rho, L) \sim \text{const.} \tag{24}$$

This is indeed verified by our numerical data [see the bottom panel of Fig. 6(c), where the maximum has been evaluated by a quadratic fit of the peak region]. We conclude that the cluster maximum linear extension d shows no finite-size scaling, apart from finite-size corrections in its density dependence.

D. Anisotropic percolation exponents

Our estimates for the Toner-Tu phase percolation exponents in two spatial dimensions, as measured from simulations of the Vicsek model, are summarized in Table I

In the Toner-Tu theory, anisotropy is controlled by the exponent ξ [8], so that one should expect $\nu_\perp = \nu_\parallel/\xi$ or

$$\xi = \frac{\nu_\parallel}{\nu_\perp} \approx 0.6 \sim 0.75. \tag{25}$$

In two spatial dimensions, based on some renormalization group conjectures, Toner and Tu suggested [37,50] that $\xi = 3/5$, a value which coincides with the lower bound of our FSS measure. However, it should be noted that the more reliable spanning estimates rather support the upper bound of our estimates $\xi \approx 0.75$, thus suggesting a less severe anisotropy. More precise measures will be required to shed light on this issue [49].

Before concluding this section, we briefly comment on the behavior of the percolation threshold as a function of the Vicsek noise amplitude η. While a careful determination of the full percolation line is beyond the scope of this work, preliminary simulations indicates that for $\eta = 0.1$ one has $\rho_c^\infty = 2.2(1)$ (see Fig. 1), suggesting that the percolation critical density in the TT phase should be a decreasing function of noise amplitude.

While this shift in the percolation threshold and in the critical exponents values may be ultimately traced back to the spontaneous symmetry breaking taking place in the Toner and Tu phase, it should be noted that in the percolation literature it is known that also an external ordering field may alter (albeit in a different way) the nature and location of the percolation point [51,52].

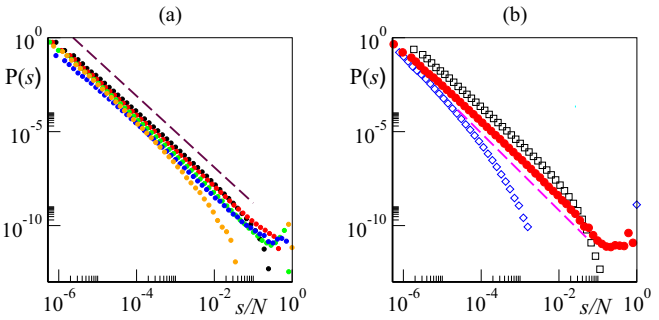

FIG. 7. (a) Cluster-size distribution $P(s)$ vs the rescaled cluster-size s/N at different densities in the Toner-Tu ordered phase (from top to bottom: $\rho = 1.3$ (black), $\rho = 1.6$ (red), $\rho = 1.9$ (green), $\rho = 2.2$ (blue), $\rho = 2.5$ (orange). The dashed line marks marks a power-law decay with a exponent equal to -1.9. (b) $P(s)$ at the percolation threshold ($\rho = 1.95$, full red circles), compared with off-critical values $\rho = 1$ (black squares) and $\rho = 4$ (blue diamonds) for $L = 1024$. The magenta dashed line marks a power-law decay with the Fisher exponent $\tau_F = 187/91 \simeq 2.0549$. All distributions are log-binned, and have been computed sampling a 10^6 time steps trajectory every 100 time steps. Other parameters: $L = 1024$, $\eta = 0.2$, and $v_0 = 0.5$.

V. CLUSTER-SIZE DISTRIBUTION IN THE TONER-TU LIQUID PHASE

We proceed to discuss cluster-size distributions, a widely used quantity both in percolation theory and in the literature on nonequilibrium clustering in active systems.

The cluster-size distribution (CSD) is one of the simplest objects to be computed numerically in percolation theory. One should notice though, that CSD corresponds to two different meanings in the literature. In a first approach, the CSD $P(s)$ measures the (properly normalized) number of clusters with size s one finds in given configurations. This corresponds in practice to the probability to find a cluster of size s when we pick at random one of the many clusters we identify in our dynamics. Other authors, however, prefer to work with the probability $Q(s)$ that a particle picked at random belongs to a cluster of size s. Obviously the two measures are related, $Q(s) = sP(s)$, so that the choice between the two above definitions is equivalent. In the following we consider $P(s)$. We measure it by sampling a large number (typically 10^4) of different steady-state configurations of our dynamics, obtained from a single run (after a dynamical transient has been discarded), with 100 time units separating consecutive configurations. In the following, we may also find convenient to further rescale the cluster-size s by the total number of particles N, so that we deal with a normalized cluster-size variable $s/N \leqslant 1$.

We have measured the CSD in the ordered liquid phase along the dashed blue line in the phase diagram of Fig. 1, that is, at noise amplitude $\eta = 0.2$. Our results, reported in Fig. 7(a), suggest that cluster size in the density interval $\rho \in [1.2, 2.2]$ follows a power-law-like behavior over a wide range of scales (about four decades for the size considered). This is in agreement with previous studies [10].

Considering density values further out from the percolation point, see for instance Fig. 7(b), one observes clear

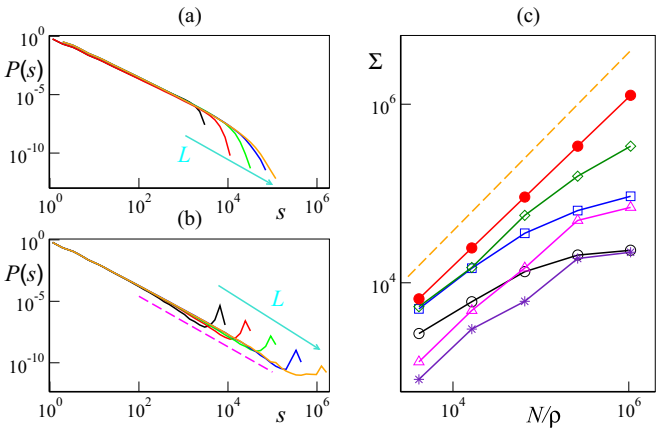

FIG. 8. (a) Finite-size variation of $P(s)$ for $\rho = 1$ (following the cyan arrow $L = 64, 128, 256, 512, 1024$). (b) same as (a), but at the percolation threshold $\rho = 1.95$, where no size-dependent cutoff is present. The magenta dashed line marks a power-law decay with the Fisher exponent $\tau_F = 187/91$. (c) Estimated cutoff length λ (see text) as a function of N/ρ for different density values: $\rho = 1$ (black circles), $\rho = 1.3$ (blue squares), $\rho = 1.6$ (green diamonds), $\rho = 1.95$ (full red circles), $\rho = 2.2$ (magenta triagles), $\rho = 2.5$ (indigo stars). The dashed orange line marks the linear relation $\sim N$. All distributions are log-binned and have been computed sampling a 10^6 time-steps trajectory every 100 time steps. Other parameters: $\eta = 0.2$ and $v_0 = 0.5$. All panels are in a double logarithmic scale.

exponential cutoffs from power-law behavior. Note that above the percolation density, $\rho > \rho_c^\infty$, where a single giant connected cluster typically appears, the CSD shows an exponential cutoff, but also, beyond that, a finite probability of observing clusters of size $s \approx N$.

The proper way to discriminate a true power-law behavior from an approximate one is, once again, finite-size analysis. We considered systems of different sizes between $L = 64$ and $L = 1024$. Off-critical CSDs, as the ones shown in Fig. 8(a), exhibit an exponential cutoff at size Σ. While Σ may initially grow with system size, finite-size analysis of its estimated value [53] shows saturation effects towards an asymptotic value $\Sigma^\infty(\rho)$. As shown in Fig. 8(c), this saturation seems to occur for all density values different from the critical percolation density, with $\Sigma^\infty(\rho)$ increasing as the percolation threshold is approached from both sides. This implies that the power laws reported in Fig. 7(a) are not asymptotic. It is only at the anisotropic percolation point $\rho \approx \rho_c^\infty = 1.96(1)$ discussed in the previous sections that $\Sigma^\infty(\rho)$ diverges, and a truly asymptotic critical CSD appears. CSDs at the percolation threshold at different system sizes are reported in Fig. 8(b). They show a large size peak corresponding to the typical size of the percolating cluster, which is clearly scaling with the system size N, as it can also be appreciated from Fig. 8(b), where we have used the location of this peak to estimate the critical point typical cluster-size Σ (full red dots).

We finally estimate the power-law-decay exponent at the percolation point. At the critical point of standard percolation, the cluster-size distribution power-law behavior is controlled by the so-called Fisher exponent,

$$\tau_F = \frac{2d_s - \beta/\nu}{d_s - \beta/\nu}, \tag{26}$$

which only depends on the spatial dimension d_s and on the critical exponents ratio β/ν [27]. In two spatial dimensions we get $\tau_F = \frac{187}{91} \approx 2.05$. We have seen that in the longitudinal percolation transition, the scaling of the largest cluster-size n is still controlled by the standard percolation exponent ratio β_p/ν_p, so that we also expect our cluster-size distribution near the critical percolation density $\rho_c^\infty \approx 1.96$ to behave as in standard percolation, that is

$$P(s) \sim s^{-\tau_F}. \tag{27}$$

This is indeed verified by our data. For $\rho = 1.95$, the corresponding CSD [full red dots in Fig. 7(b)] exhibits a power-law behavior fully compatible with the standard Fisher exponent (orange dashed line) over several decades. Our best fit, carried on over roughly four decades, gives indeed $\tau_F = 2.03(3)$. Note that this value is different from that of the apparent, non asymptotic power laws observed at $\rho \neq \rho_c^\infty$, which have been found typically in the range [1.8, 2] [10,24].

Altogether, our results show that, while truly critical CSDs only appear at the percolation point, the Toner-Tu ordered phase nevertheless displays an extended "quasicritical" region, where cluster-size distributions follow a power law over several orders of magnitudes and for a wide range of densities. This approximate critical regime has also been reported in previous works [10,24,26] and—as we have discussed in the introduction—has led some authors to speculate that the onset of collective motion should be accompanied by a percolation transition. The analysis of the anisotropic percolation transition carried on in the previous chapter, however, clarifies that the Toner-Tu phase of finite-size systems is characterized by a "double" percolation transition, with giant clusters first percolating transversally with respect to the mean direction of motion and, at higher densities, also spanning in the longitudinal direction. We conjecture that this extended region of scaling is related to the two separate finite-size transitions at two clearly different densities. Note also that far away from this "extended region," the cluster-size distributions are clearly not scale free; see, for instance, the case $\rho = 4$, $\eta = 0.2$ (blue diamonds) in Fig. 7(b).

VI. PERCOLATION AND CLUSTERING IN THE DISORDERED AND COEXISTENCE PHASES

A percolation transition is of course also found in the disordered gas phase. It is a simple isotropic one with standard exponents. Its transition line is reported in Fig. 1, and for maximal noise culminates at the well known critical point for a Poisson point process, $\rho_c^{\mathrm{PPP}} = 1.43632545(9)$, as discussed at the end of Sec. IV. Note that also in this case, the short-ranged correlations arising in the disordered phase for noise amplitudes $\eta < 1$ shift the critical percolation point to slightly larger density values. Here, however, without the "double" finite-size percolation mechanism we have unearthed in the symmetry broken regime, off-critical cluster-size distributions do not show any apparent power-law behavior as their

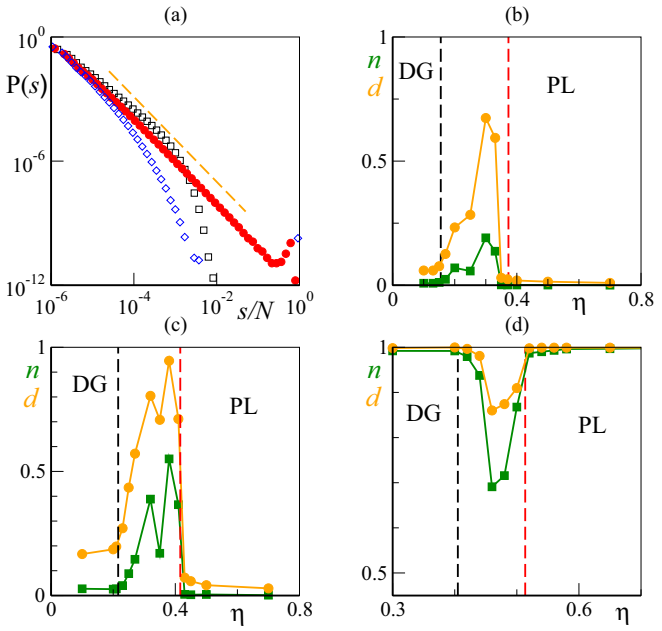

FIG. 9. (a) Cluster-size distribution P(s) vs rescaled cluster-size s/N for $\eta = 0.7$ and different densities in the disordered gas phase($L = 1024$); from top to bottom: $\rho = 1.3$ (black squares), $\rho = 1.51$ (the percolation point, full red circles), and $\rho = 1.7$ (blue diamonds). The orange dashed line marks a power-law decay with the Fisher exponent $\tau_F = 187/91$. (b), (c), (d) Mean value of the largest cluster size, n (green squares) and maximum cluster extension, d (orange circles) vs noise amplitude η across all three phases. Parameters: $v_0 = 0.5$ and (b) $L = 1024$, $\rho = 0.5$, (c) $L = 1024$, $\rho = 1$, (d) $L = 512$, $\rho = 4$. The black vertical dashed lines mark the finite-size onset of order [54], $\eta = \eta_{\rm gas}(L)$, while the red ones, at $\eta = \eta_{\rm liq}$, separate phase coexistence (between the two vertical lines) from the Toner-Tu polar liquid (PL).

counterparts in the ordered liquid phase. See, for instance, Fig. 9(a) for noise amplitude $\eta = 0.7$

In the coexistence phase delimited by the two binodal lines, where high-density high-order traveling bands are observed, the cluster dynamics is radically different. We selected three different densities well below ($\rho = 0.5$, $\rho = 1$) and above ($\rho = 4$) the percolation transition lines of both the disordered gas and the Toner-Tu phases, and varied the noise amplitude as shown in Fig. 1, to cut across both binodals. We computed both the largest cluster size, n and the maximum cluster extension, d. For low densities, data shows that in the gas and Toner-Tu phases, clusters are small and do not reach a macroscopic, system spanning state [Figs. 9(b) and 9(c)]. However, in the coexistence region [54], high and low local density patches appear (signaling the presence of ordered liquid bands traveling in a disordered gas) [35], and system spanning clusters suddenly appear. However, at large densities [Fig. 9(d)], in both the gas and Toner-Tu phases, one has typically a single cluster encompassing almost all particles, with $n, d \approx 1$. The appearance of lower density disordered patches, however, induces a drop in the maximum cluster size in the coexistence region. It has been shown that, due to these effects, also the cluster-size distribution built by averaging over both phases in the coexistence region show apparent power laws, albeit with a decay exponent larger than the Fisher one [10].

VII. DISCUSSION AND CONCLUSIONS

Our numerical results show that nonequilibrium clustering effects in the two-dimensional Vicsek model are essentially controlled by an underlying percolation point and are therefore mainly geometrical in nature. Cluster dynamics and cluster-size distributions behave differently, not only in the different phases but also within phases, as one always expects to cross a percolation transition when the density is sufficiently large. Moreover, crossing one of the binodal lines delimiting the coexistence phase separating the disordered gas from the Toner-Tu ordered liquid, sudden changes are typically observed in the cluster dynamics and corresponding cluster-size distributions. These transitions, however, are dictated by the overall phase-separation scenario of the phase diagram, and not vice versa.

In the disordered gas phase, a standard percolation transition is observed, akin to that observed at maximal noise (i.e., in a system fully equivalent to a Poisson point process), with standard percolation exponents [27] but a slight shift in the critical percolation density due to short-range correlations.

In the Toner-Tu symmetry-broken phase, however, we have identified an anisotropic percolation transition with clusters first spanning the transversal direction (with respect to the mean direction of motion) and only later, at higher densities, spanning also along the longitudinal direction. A careful finite-size analysis revealed that these two distinct percolation thresholds seem to converge to the same density value in the thermodynamic limit, albeit with two different correlation exponents $\nu_\perp$ and $\nu_\parallel$, which are are also clearly different from the well-known value of the standard percolation correlation exponent ν_p in two spatial dimensions.

We have argued that the difference in the correlation exponents can be attributed to the long-range correlations which characterize density fluctuations in the Toner-Tu phase. In particular, making use of the Harris criterion [47] for correlated percolation, we have been able to link the value of the longitudinal correlation exponent (the one controlling the onset of a cluster of macroscopic mass spanning in both directions) with the isotropic (i.e., averaged over all directions) density fluctuation correlations.

The hyperscaling relation of standard percolation seems to hold also in the correlated Toner-Tu phase, with the key exponents controlling the cluster-size distribution (the Fisher exponent τ_F) and the first two momenta of the maximum cluster size (β/ν and γ/ν) compatible with their values from standard percolation theory.

In general, it is only at the percolation point that the cluster-size distribution is truly scale free ($P(s) \sim s^{-\tau_F}$). However, cluster-size distributions resembling power laws over a wide range of scales occur for a finite range of densities in the Toner-Tu phase, presumably because of the "double-threshold" mechanism of anisotropic percolation. Only a careful finite-size analysis can show that

these power laws are not asymptotic but bounded by a size-independent cutoff.

Here we have closely analyzed clustering and percolation in the classical Vicsek model for flocking, but we expect our main conclusions to be generic and to hold in the more general context of dry aligning active matter.

ACKNOWLEDGMENTS

We have benefited from discussions with F. Perez-Reche. N.K. and F.G. acknowledge support from the Marie Curie Career Integration Grant No. PCIG13-GA-2013-618399. F.G. also acknowledges support from EPSRC First Grant No. EP/K018450/1.

[1] S. Ramaswamy, Ann. Rev. Cond. Matt. Phys. **1**, 323 (2010).
[2] M. Ballerini *et al.*, Proc. Natl. Acad. Sci. USA **105**, 1232 (2008).
[3] N. Sepúlveda, L. Petitjean, O. Cochet, E. Grasland-Mongrain, P. Silberzan, and V. Hakim, PLoS Comput. Biol. **9**, e1002944 (2014).
[4] X. Trepat, M. R. Wasserman, T. E. Angelini, E. Millet, D. A. Weitz, J. P. Butler, and J. J. Fredberg, Nat. Phys. **5**, 426 (2009).
[5] V. Schaller, C. Weber, C. Semmrich, E. Frey, and A. R. Bausch, Nature **467**, 73 (2010).
[6] J. Palacci, S. Sacanna, A. Preska Steinberg, D. J. Pine, and P. M. Chaikin, Science **339**, 936 (2013).
[7] T. Vicsek, A. Czirók, E. Ben-Jacob, I. Cohen, and O. Shochet, Phys. Rev. Lett. **75**, 1226 (1995).
[8] J. Toner and Y. Tu, Phys. Rev. Lett. **75**, 4326 (1995).
[9] S. Ramaswamy, R. A. Simha, and J. Toner, Europhys. Lett. **62**, 196 (2003).
[10] H. Chaté, F. Ginelli, G. Grégoire, and F. Raynaud, Phys. Rev. E **77**, 046113 (2008).
[11] A. Cavagna, A. Cimarelli, I. Giardina, G. Parisi, R. Santagati, F. Stefanini, and M. Viale, Proc. Natl. Acad. Sci. USA **107**, 11865 (2010).
[12] F. Giavazzi, C. Malinverno, S. Corallino, F. Ginelli, G. Scita, and R. Cerbino, J. Phys. D: Appl. Phys. **50**, 384003 (2017).
[13] H. P. Zhang, A. Beer, E. L. Florin, and H. L. Swinney, Proc. Natl. Acad. Sci. USA **107**, 13626 (2010).
[14] S. Köler, V. Schaller, and A. Bausch, Nat. Mater. **10**, 462 (2011).
[15] L. Huber, R. Suzuki, T. Krüger, E. Frey, and A. R. Bausch, Science **361**, 255 (2018).
[16] F. Ginelli, F. Peruani, M.-H. Pillot, H. Chaté, G. Theraulaz, and R. Bon, Proc. Natl. Acad. Sci. USA **112**, 12729 (2015).
[17] I. Theurkauff, C. Cottin-Bizonne, J. Palacci, C. Ybert, and L. Bocquet, Phys. Rev. Lett. **108**, 268303 (2012)
[18] F. Peruani, J. Starruß, V. Jakovljevic, L. Søgaard-Andersen, A. Deutsch, and M. Bär, Phys. Rev. Lett. **108**, 098102 (2012).
[19] F. Peruani, A. Deutsch, and M. Bär, Phys. Rev. E **74**, 030904(R) (2006).
[20] Y. Yang, V. Marceau, and G. Gompper, Phys. Rev. E **82**, 031904 (2010).
[21] M. Abkenar, K. Marx, T. Auth, and G. Gompper, Phys. Rev. E **88**, 062314 (2013).
[22] E. Tjhung, C. Nardini, and M. E. Cates, Phys. Rev. X **8**, 031080 (2018).
[23] X.-q. Shi and H. Chaté, arXiv:1807.00294.
[24] C. Huepe and M. Aldana, Phys. Rev. Lett. **92**, 168701 (2004).
[25] F. Peruani, L. Schimansky-Geier, and M. Bär, Eur. Phys. J. Spec. Top. **157**, 111 (2008).
[26] F. Peruani and M. Bär, New J. Phys. **15**, 065009 (2013).
[27] D. Stauffer and A. Aharony, *Introduction to Percolation Theory*, revised 2nd ed. (Taylor & Francis, London 1994).
[28] For a recent review, see H. Chaté, Ann. Rev. Cond. Mat. Phys (unpublished).
[29] A. P. Solon and H. Chaté, and J. Tailleur Phys. Rev. Lett. **114**, 068101 (2015).
[30] Both the interaction range and the time step can be rescaled to unit values without any loss of generality.
[31] A. Gabrielli, F. Sylos Labini, M. Joyce, and L. Pietronero, *Statistical Physics for Cosmic Structures* (Springer Verlag, New York/Berlin, 2005).
[32] G. Grégoire and H. Chaté, Phys. Rev. Lett. **92**, 025702 (2004).
[33] E. Bertin, M. Droz, and G. Grégoire, J. Phys. A **42**, 445001 (2009).
[34] T. Ihle, Phys. Rev. E **83**, 030901(R) (2011).
[35] A. P. Solon, J. B. Caussin, D. Bartolo, H. Chaté, and J. Tailleur, Phys. Rev. E **92**, 062111 (2015).
[36] F. Ginelli, Eur. Phys. J. ST **225**, 2099 (2016).
[37] Y. Tu, J. Toner, and M. Ulm, Phys. Rev. Lett. **80**, 4819 (1998).
[38] This is numerically much faster (order s vs order s^2 in a cluster of s particles) to compute than the maximum distance between any couple of particles in the cluster. Of course, periodic boundary conditions are properly taken into account computing the cluster center of mass.
[39] D. Levis and L. Berthier, Phys. Rev. E **89**, 062301 (2014).
[40] In practice, for each configuration we first verify which of the two cartesian axes forms the smaller angle with the instantaneous direction of motion $\mathbf{V}(t)$. This will be the longitudinal axis, and the two opposite sides of our square system joined by the longitudinal axis are the the longitudinal sides. Likewise, the remaining axis and opposite sides are the transversal ones. Clusters spanning from one longitudinal (transversal) side to the other are longitudinal (transversal) spanning clusters, and we evaluate the longitudinal (transversal) spanning probability as the frequency of instantaneous system configurations with at least one longitudinal (transversal) spanning cluster.
[41] We measure the autocorrelation time τ as the time needed for the autocorrelation function to drop to 10% of its equal time value.
[42] *Finite Size Scaling and Numerical Simulations of Statistical Systems*, edited by V. Privman (World Scientific, Singapore, 1990).
[43] D. W. Heermann and D. Stauffer, Z. Physik B **40**, 133 (1980).
[44] A. A. Saberi, Phys Rep. **578**, 1 (2015).
[45] More precisely, we fit $S_2(\rho)$ by $F(\rho) \equiv \{1 - \mathrm{erf}[a_1(\rho - a_0)]\}/2$, with the size-dependent fitting parameters a_0 and a_1. Obviously, $\rho_c(L) = a_0$.
[46] S. Mertens and C. Moore, Phys. Rev. E **86**, 061109 (2012).

[47] A. B. Harris, J. Phys. C **7**, 1671 (1974).
[48] A. Weinrib, Phys. Rev. B **29**, 387 (1984).
[49] B. Mahault, F. Ginelli, and H. Chaté (unpublished).
[50] J. Toner, Phys. Rev. E **86**, 031918 (2012).
[51] R. H. J. Otten and P. van der Schoot, Phys. Rev. Lett. **108**, 088301 (2012).
[52] S. P. Finner, M. I. Kotsev, M. A. Miller, and P. van der Schoot, J. Chem. Phys. **148**, 034903 (2018)
[53] To estimate the off-critical cut-of-size Σ from the CSD, we first subtract the apparent power-law decay. Σ correspond to the cluster size at which this rescaled CSD drops below the threshold $1/e$. We have verified that the choice of different thresholds does not change the qualitative picture.
[54] For a better comparison with our finite-size clustering measures, here we have characterized the symmetry-breaking transition between the disordered gas and the coexistence region by its appropriate finite-size value [10] rather than by the more rigorous binodal value.